ChemComm

# Photophysical characterization of a highly luminescent divalent-europium-containing azacryptate



| | |
|---|---|
| Journal: | *ChemComm* |
| Manuscript ID | CC-COM-03-2018-001737.R1 |
| Article Type: | Communication |
| | |



Journal Name

COMMUNICATION

# Photophysical characterization of a highly luminescent divalent-europium-containing azacryptate

Received 00th January 20xx,
Accepted 00th January 20xx

DOI: 10.1039/x0xx00000x

www.rsc.org/

Tyler C. Jenks,[a] Matthew D. Bailey,[a] Brooke A. Corbin,[a] Akhila N. W. Kuda-Wedagedara,[a] Philip D. Martin,[b] H. Bernhard Schlegel,[a,*] Federico A. Rabuffetti[a,*] and Matthew J. Allen[a,*]

**We report a new luminescent $Eu^{II}$-containing complex. The complex is excited with visible light, leading to emission centered at 447 nm with a lifetime of 1.25 μs. Computational studies suggest that the steric bulk of the ligand is a major factor influencing the wavelength of emission.**

Luminescent materials and complexes have numerous applications in displays,[1] lighting,[2] imaging,[3] sensing,[4] and catalysis.[5–6] Two of the most desirable traits for luminescent materials are tunability and high quantum efficiency. Recently, a highly efficient $Eu^{II}$-containing complex, Eu**1**$Cl_2$ (Figure 1), was reported that displayed yellow luminescence with a bathochromic shift from typical $Eu^{II}$-based excitations and emissions to the visible region of the electromagnetic spectrum.[7] These large shifts prompted us to explore the ligand-induced tunability of emission for $Eu^{II}$. Here, we report a new $Eu^{II}$-containing complex that advances the understanding of the effect of ligand design on the enhancement and tunability of $Eu^{II}$ luminescence in solution.

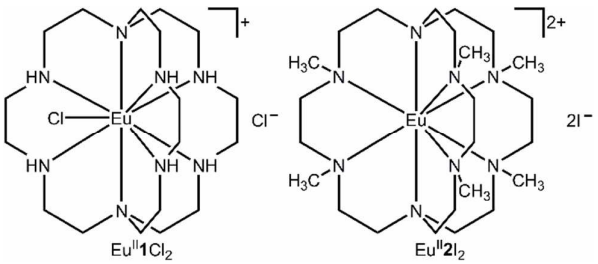


**Fig. 1** Structures of (left) Eu**1**$Cl_2$ and (right) Eu**2**$I_2$.

Our design was based on experimental and computational studies that demonstrated that an increased splitting of 5d-orbital energies results in decreased f–d transition energies.[7–8] The influence of a strong-field ligand on f–d transitions was demonstrated by the bathochromic shift observed with Eu**1**$Cl_2$ relative to a $Eu^{II}$-containing [2.2.2]-cryptate.[7,9] We hypothesized that conversion of the secondary amine donors of Eu**1**$Cl_2$ to tertiary amines would increase the ligand field splitting of the 5d orbitals, inducing a smaller f–d transition energy and a further red-shifted emission.

The conversion of secondary amines on ligand **1** to the tertiary amines of ligand **2** was accomplished following a reported procedure that used an Eschweiler–Clarke reaction to functionalize the secondary amines with methyl groups.[10] Hexamethylated ligand **2** was metalated by mixing solutions of $EuI_2$ and **2** in tetrahydrofuran, resulting in the precipitation of Eu**2**$I_2$. Complex Eu**2**$I_2$ is soluble and luminescent in degassed water, but attempts at crystallization from water were unsuccessful. However, vapor diffusion of tetrahydrofuran into a concentrated methanolic solution of Eu**2**$I_2$ yielded yellow crystals that were suitable for X-ray diffraction.

X-ray crystallography was performed to explore the geometry of Eu**2**$I_2$, revealing a unit cell containing four dicationic units of $[Eu\mathbf{2}]^{2+}$, eight outer-sphere iodide ions, and four disordered outer-sphere molecules of methanol (Figure 2). The europium ion is coordinated by each tertiary nitrogen atom of the ligand in a distorted bicapped trigonal antiprism, and Eu–N bond lengths are between 2.822 and 2.975 Å, which are within the expected range for divalent europium with tertiary amines.[6–7,11–12] When viewing the complex along the $C_3$ axis (Figure 2, right), the three anterior methyl groups are oriented in the opposite direction as the three posterior methyl groups. As a result of this orientation, two methyl groups from adjacent arms are situated in front of the $Eu^{II}$ ion between each pair of arms of the cryptate. These methyl groups sterically block the sites at which anions or solvent molecules coordinate to $Eu^{II}$ in other cryptates.[7,12] Unlike Eu**1**$Cl_2$ that contains one inner-sphere chloride, Eu**2**$I_2$ has no inner-sphere anions or solvent molecules, likely due to the alignment of the methyl groups. However, because of the difference in anions between Eu**1**$Cl_2$ and Eu**2**$I_2$, we could not rule

[a] *Department of Chemistry, Wayne State University, 5101 Cass Avenue, Detroit, MI, 48202, USA. Email: hbs@chem.wayne.edu, far@chem.wayne.edu, mallen@chem.wayne.edu*
[b] *Lumigen Instrument Center, Department of Chemistry, Wayne State University, 5101 Cass Avenue, Detroit, MI, 48202, USA.*
Electronic Supplementary Information (ESI) available: experimental procedures, synthesis and crystallographic data for Eu**1**$I_2$ and Eu**2**$I_2$, and computational data (.pdf file) and computed Cartesian coordinates (.xyz files). See DOI: 10.1039/x0xx00000x

out the possibility that the larger iodide anion precluded coordination instead of the methyl groups.

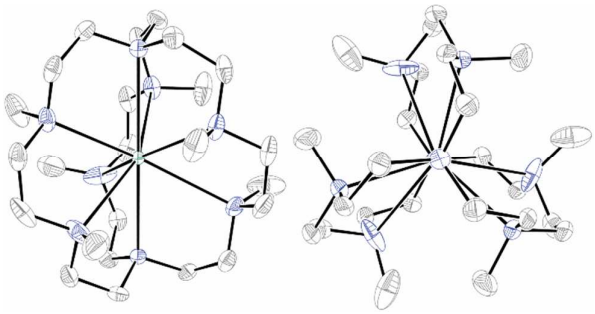

**Fig. 2** Crystal structure of Eu**2**$I_2$ oriented (left) perpendicular to and (right) along the $C_3$ axis. Hydrogen atoms, two outer-sphere iodide ions, and one molecule of methanol are omitted for clarity. Thermal ellipsoids are drawn at 50% probability. Crystallographic data for this structure are available at the Cambridge Crystallographic Data Centre under deposition number CCDC 1826978. Blue = nitrogen; grey = carbon; and seagreen = europium.

To study the relative influence of methyl groups and counteranions on geometry, we crystallized Eu**1**$I_2$. The structure of Eu**1**$I_2$ revealed a similar nine-coordinate hula-hoop geometry as Eu**1**$Cl_2$ with iodide replacing chloride (Figure 3).[7] The iodide structure indicates that the methyl groups, and not the size of the anion, were responsible for the change in coordination of Eu**2**$I_2$ relative to Eu**1**$Cl_2$ or Eu**1**$I_2$. After observing the structural features of Eu**2**$I_2$, we characterized its photophysical properties.

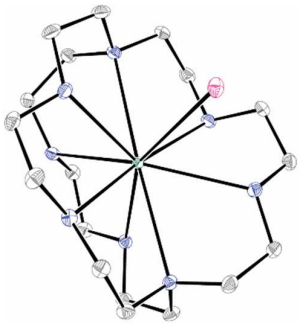

**Fig. 3** Crystal structure of Eu**1**$I_2$. Hydrogen atoms and an outer-sphere iodide ion have been omitted for clarity. Thermal ellipsoids are drawn at 50% probability. Crystallographic data for this structure are available at the Cambridge Crystallographic Data Centre under deposition number CCDC 1826977. Blue = nitrogen; grey = carbon; seagreen = europium; and pink = iodine.

To probe the photophysical properties of Eu**2**$I_2$, absorption, excitation, and emission spectra were collected (Figure 4). Solutions of Eu**2**$I_2$ were handled under inert atmosphere because luminescence decreased in the presence of air, likely due to oxidation of $Eu^{II}$ to $Eu^{III}$. The UV–visible spectrum showed two absorbance peaks centered at 261 ($\varepsilon$ = 752 $M^{-1}$ $cm^{-1}$) and 345 nm ($\varepsilon$ = 274 $M^{-1}$ $cm^{-1}$). Luminescence studies revealed a broad excitation peak at 271 nm and another centered at 349 nm that trailed into the visible region, with an associated broad emission peak centered at 447 nm. These broad peaks are indicative of f–d transitions.[8–9,13] With the addition of the electron-donating methyl groups to the coordinating nitrogen atoms of the cryptand, we expected to see a bathochromic shift in the absorbance of Eu**2**$I_2$ relative to Eu**1**$Cl_2$. This shift was expected because an increased splitting of the d-orbitals by the stronger-field tertiary amine donors of **2** relative to the secondary amine donors of **1** should result in a lower-energy f–d transition for $Eu^{II}$. Instead, we observed a slight hypsochromic shift that brought the absorbance of Eu**2**$I_2$ to the high-energy edge of the visible region. We suspected that this shift was due to the change in geometry of Eu**2**$I_2$ relative to Eu**1**$Cl_2$ overpowering the splitting differences, similar to what would be expected when moving between octahedral and tetrahedral geometries.

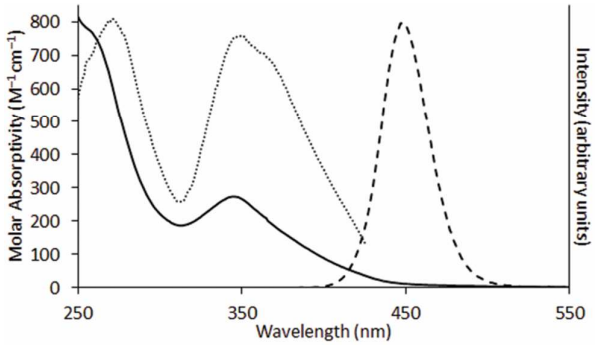


**Fig. 4** Absorption (—, left *y*-axis), excitation (··, right *y*-axis), and emission (--, right *y*-axis) spectra of Eu**2**$I_2$ (1.8 mM) in methanol.

To support our proposed explanation for the hypsochromic shift, we employed time-dependent density functional theory (TD-DFT) calculations to identify the molecular orbitals involved in the luminescence of $[Eu\mathbf{2}]^{2+}$. Prior to TD-DFT calculations, geometry optimization calculations were performed to compare the calculated ground-state geometry in solution to the solid-state crystallographic coordinates. After optimization of $[Eu\mathbf{2}]^{2+}$ with the SMD implicit solvation model in methanol, the Eu–N bond distances from the calculation (2.893–3.145 Å) were found to be in good agreement with crystallographic bond distances (2.822–2.975 Å) (Table S3).[8,14] With the completion of the ground state optimization, the calculation for $[Eu\mathbf{2}]^{2+}$ ground-state geometry was validated, and excitation and emission calculations were pursued.

TD-DFT calculations (80 states)[8,15] were performed to obtain simulated excitation and emission spectra of $[Eu\mathbf{2}]^{2+}$. The calculated absorbance spectrum (Figure S4) displays two broad peaks centered at 268 and 357 nm that are comparable to the broad peaks in the experimental spectrum centered at 261 and 345 nm. To simulate the emissive state, we optimized the geometry corresponding to the high-oscillator-strength transition from the lower-energy absorbance curve. TD-DFT calculations of the emissive state were then employed to simulate the emission.[15] The calculated emission spectrum (Figure S5) displayed a maximum value at 384 nm and is within the expected error of the experimental value (447 nm).[8] To further understand the luminescence, natural-transition-orbital calculations were performed to characterize the high-oscillator-strength transitions involved in the two major excitations. For the

high-energy excitation at 268 nm, natural-transition-orbital calculations revealed an expected 4f–5d transition, specifically from a $4f_z^3$-type orbital to a $5d_z^2$-type orbital with an oscillator strength of 0.029. For the lower-energy excitation at 357 nm, natural-transition-orbital calculations revealed a 4f–5d transition from a 4f-type orbital to a $5d_{xy}$-type orbital with an oscillator strength of 0.0036. Comparison of the TD-DFT and natural-transition-orbital calculations of $[Eu\mathbf{2}]^{2+}$ to reported calculations of $[Eu\mathbf{1}Cl]^{+}$ revealed that both complexes involve similar orbital transitions for both the high and low energy excitations.[8] Because the orbitals involved in the transitions for both $[Eu\mathbf{1}Cl]^{+}$ and $[Eu\mathbf{2}]^{2+}$ are similar, we sought to use an orbital energy diagram to compare the relative changes in orbital splitting energies. The orbital-energy diagrams for $[Eu\mathbf{1}Cl]^{+}$ and $[Eu\mathbf{2}]^{2+}$ based on these calculations (Figure 5) are consistent with our measurements but display d-orbital splitting opposite to what would be expected based solely on the change from secondary to tertiary amines.

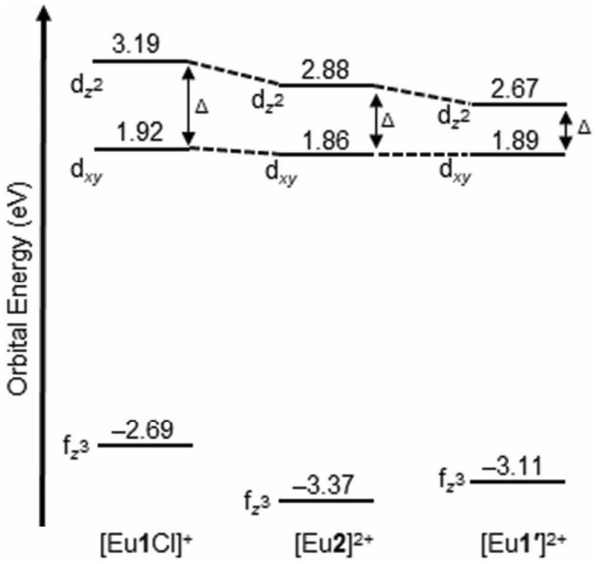


**Fig. 5** Orbital-energy diagram for the $5d_z^2$, $5d_{xy}$, and $4f_z^3$ orbitals for (left) $[Eu\mathbf{1}Cl]^{+}$,[8] (middle) $[Eu\mathbf{2}]^{2+}$, and (right) $[Eu\mathbf{1'}]^{2+}$ (where $[Eu\mathbf{1'}]^{2+}$ is $[Eu\mathbf{1}Cl]^{+}$ forced into an eight-coordinate distorted bicapped antiprism, like $[Eu\mathbf{2}]^{2+}$). Dashed lines are visual guides.

To better understand the impact of the different intramolecular factors contributing to the orbital energies, we developed a computational control experiment in which we forced $[Eu\mathbf{1}Cl]^{+}$ to adopt an eight-coordinate distorted bicapped antiprism like $[Eu\mathbf{2}]^{2+}$, and we calculated the excitation of the new complex, $[Eu\mathbf{1'}]^{2+}$. Upon optimization and subsequent TD-DFT calculations, we found the orbital energies for $[Eu\mathbf{1'}]^{2+}$ to be different from the reported values for $[Eu\mathbf{1}Cl]^{+}$ in two distinct ways (Figure 5): The change from nine-coordinate to eight-coordinate geometries lowered the energy of the 4f orbitals and decreased the splitting of the 5d orbital energies. Further, comparison of the calculations for $[Eu\mathbf{2}]^{2+}$ and $[Eu\mathbf{1'}]^{2+}$ revealed that the d-orbital splitting supported our original hypothesis regarding expected trends based on the spectrochemical series: a smaller splitting energy was observed with the secondary-amine donors of $[Eu\mathbf{1'}]^{2+}$ relative to the tertiary-amine donors of $[Eu\mathbf{2}]^{2+}$. From these calculations, we conclude that the cause of the observed hypsochromic shift in emission of $Eu\mathbf{2}I_2$ relative to $Eu\mathbf{1}Cl_2$ is dominated by the change in geometry and coordination number.

While characterizing the photophysical properties of $Eu\mathbf{2}I_2$, we noticed that the luminescence of a solution of $Eu\mathbf{2}I_2$ in methanol was visible to the unaided eye in ambient (laboratory fluorescent) light (Figure 6). Against a white background, the solution appeared pale yellow, but when viewed against a black background, the solution appeared blue. The color difference was rationalized with the assumption that light is reflected off a white surface but absorbed by a black surface. The reflected light is absorbed by the solution resulting in the transmission of yellow light. Without reflected light (black background), only blue luminescence is visible. The visible luminescence with ambient-light excitation led us to expect a large quantum yield for $Eu\mathbf{2}I_2$ in methanol and prompted us to characterize the excited state by the measuring quantum yield and luminescence lifetime. Using an integrating sphere, the quantum yields of four dilute samples (roughly 0.2, 0.4, 0.6, and 1 mM) of $Eu\mathbf{2}I_2$ in methanol were measured, giving a value of 47 ± 3%.[‡] This quantum yield is among the largest of any discrete $Eu^{II}$-containing complex in solution, and is, to the best of our knowledge, the largest in a protic solvent. The lifetime of the excited state of $Eu\mathbf{2}I_2$ was also measured in methanol and was found to be 1.25 μs, which is within the expected range for $Eu^{II}$-containing complexes.[6,13,16] Because interactions with O–H or N–H oscillators from solvent molecules or ligands cause non-radiative decay of $Eu^{II}$ excited states,[7,9,13] the efficient luminescence of $Eu\mathbf{2}I_2$ in methanol is likely due to two aspects of the cryptand: the lack of N–H oscillators on the ligand and the steric shielding of the $Eu^{II}$ ion from solvent molecules by the methyl groups. Relative to $Eu\mathbf{1}Cl_2$, the lack of space for inner-sphere coordination and lack of ligand-based N–H oscillators results in fewer vibrational modes that quench the excited state of $Eu\mathbf{2}I_2$ via non-radiative decay.

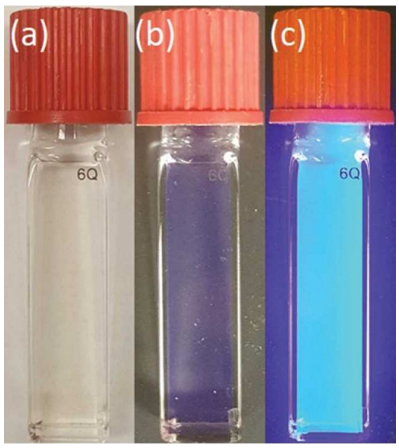


**Fig. 6** Quartz cuvette (1 cm path length) containing a solution of $Eu\mathbf{2}I_2$ (1.5 mM) in methanol with (a) white and (b) black backgrounds. (c) The same cuvette under irradiation from a long-wave UV handheld lamp.

## Conclusions

In conclusion, we have described a new $Eu^{II}$-containing complex that displays blue luminescence with a high quantum efficiency in protic solvent. This efficiency stems from the steric bulk of the methyl groups and lack of N–H oscillators. Crystal structures and TD-DFT calculations indicated that the blue emission is due to geometry having a larger influence on electronic transitions than d-orbital splitting from the ligand environment. This cryptate provides insight into the role of sterics and coordination environment that is expected to be useful for the rational design of divalent-lanthanide-containing complexes with desirable photophysical properties.

This work was supported by the National Science Foundation (CHE-1564755). M.D.B. is thankful for a Rumble Fellowship (Wayne State University). We also thank the Wayne State University computing grid for the computational time.

## Conflicts of interest

There are no conflicts to declare.

## Notes and references

‡ Values are reported as mean ± standard error of the mean.

1 Z. Zhang, B. Xu, J. Su, L. Shen, Y. Xie and H. Tian, *Angew. Chem. Int. Ed.*, 2011, **50**, 11654; Y. Sagara and T. Kato, *Angew. Chem.*, 2011, **123**, 9294; J. H. Kang, J. Y. Kim and D. Y. Jeon, *J. Electrochem. Soc.*, 2005, **152**, H33; T. Sun, X. Chen, L. Jin, H.-W. Li, B. Chen, B. Fan, B. Moine, X. Qiao, X. Fan, S.-W. Tsang, S. F. Yu and F. Wang, *J. Phys. Chem. Lett.*, 2017, **8**, 5099; A. de Bettencourt-Dias and J. S. K. Rossini, *Inorg. Chem.*, 2016, **55**, 9954.

2 Y. Wei, Q. Li, R. Sa and K. Wu, *Chem. Commun.*, 2014, **50**, 1820; K. Singh, R. Boddula and S. Vaidyanathan, *Inorg. Chem.*, 2017, **56**, 9376; W. Wu and Z. Xia, *RSC Adv.*, 2013, **3**, 6051; R. Yu, H. M. Noh, B. K. Moon, B. C. Choi, J. H. Jeong, K. Jang, S. S. Yi and J. K. Jang, *J. Alloys Compd.*, 2013, **576**, 236; A. A. Setlur, W. J. Heward, Y. Gao, A. M. Srivastava, R. G. Chandran and M. V. Shankar, *Chem. Mater.*, 2006, **18**, 3314.

3 J. Liu, J. Bu, W. Bu, S. Zhang, L. Pan, W. Fan, F. Chen, L. Zhou, W. Peng, K. Zhao, J. Du and J. Shi, *Angew. Chem. Int. Ed.*, 2014, **53**, 4551; K. Hanaoka, K. Kikuchi, S. Kobayashi and T. Nagano, *J. Am. Chem. Soc.*, 2007, **129**, 13502; E. Debroye and T. N. Parac-Vogt, *Chem. Soc. Rev.*, 2014, **43**, 8178; J.-C. G. Bünzli, *Chem. Rev.*, 2010, **110**, 2729.

4 M. Jin, T. Sumitani, H. Sato, T. Seki and H. Ito, *J. Am. Chem. Soc.*, 2018, **140**, 2875; K. Y. Zhang, Q. Yu, H. Wei, S. Liu, Q. Zhao and W. Huang, *Chem. Rev.*, 2018, **118**, 1770; S. J. Bradberry, A. J. Savyasachi, M. Martinez-Calvo and T. Gunnlaugsson, *Coord. Chem. Rev.*, 2014, **273–274**, 226; S. V. Eliseeva and J.-C. G. Bünzli, *Chem. Soc. Rev.*, 2010, **39**, 189; I. L. V. Rosa, F. A. Tavares, A. P. de Moura, I. M. Pinatti, L. F. da Silva, M. S. Li and E. Longo, *J. Lumin.*, 2018, **197**, 38; J. D. Moore, R. L. Lord, G. A. Cisneros and M. J. Allen, *J. Am. Chem. Soc.*, 2012, **134**, 17372; T. Liu, A. Nonat, M. Beyler, M. Regueiro-Figueroa, K. N. Nono, O. Jeannin, F. Camerel, F. Debaene, S. Cianférani-Sanglier, R. Tripier, C. Platas-Iglesias and L. J. Charbonnière, *Angew. Chem. Int. Ed.*, 2014, **53**, 7259.

5 H. Yin, Y. Jin, J. E. Hertzog, K. C. Mullane, P. J. Carroll, B. C. Manor, J. M. Anna and E. J. Schelter, *J. Am. Chem. Soc.*, 2016, **138**, 16266; J. J. Devery, III, J. D. Nguyen, C. Dai and C. R. J. Stephenson, *ACS Catal.*, 2016, **6**, 5962; S. Lin, S. D. Lies, C. S. Gravatt and T. P. Yoon, *Org. Lett.*, 2017, **19**, 368; D. A. Nicewicz and D. W. C. MacMillan, *Science*, 2008, **322**, 77; J. J. Devery, III, J. J. Douglas, J. D. Nguyen, K. P. Cole, R. A. Flowers, II and C. R. J. Stephenson, *Chem. Sci.*, 2015, **6**, 537; P. Dissanayake, M. J. Allen, *J. Am. Chem. Soc.*, 2009, **131**, 6342; P. Dissanayake, Y. Mei, M. J. Allen, *ACS Catal.*, 2011, **1**, 1203.

6 T. C. Jenks, M. D. Bailey, J. L. Hovey, S. Fernando, G. Basnayake, M. E. Cross, W. Li and M. J. Allen, *Chem. Sci.*, 2018, **9**, 1273.

7 A. N. W. Kuda-Wedagedara, C. Wang, P. D. Martin and M. J. Allen, *J. Am. Chem. Soc.*, 2015, **137**, 4960.

8 B. A. Corbin, J. L. Hovey, B. Thapa, H. B. Schlegel and M. J. Allen, *J. Organomet. Chem.*, 2018, **857**, 88.

9 N. Sabbatini, M. Ciano, S. Dellonte, A. Bonazzi, F. Bolletta and V. Balzani, *J. Phys. Chem.*, 1984, **88**, 1534.

10 D. Farrell, C. J. Harding, V. McKee and J. Nelson, *Dalton Trans.*, 2006, 3204.

11 L. A. Basal, M. D. Bailey, J. Romero, M. M. Ali, L. Kurenbekova, J. Yustein, R. G. Pautler and M. J. Allen, *Chem. Sci.*, 2017, **8**, 8345; K. Müller-Buschbaum, Y. Mokaddem, F. M. Schappacher and R. Pöttgen, *Angew. Chem. Int. Ed.*, 2007, **46**, 4385; L. Burai, É. Tóth, S. Seibig, R. Scopelliti and A. E. Merbach, *Chem. Eur. J.*, 2000, **6**, 3761.

12 C. U. Lenora, F. Carniato, Y. Shen, Z. Latif, E. M. Haacke, P. D. Martin, M. Botta and M. J. Allen, *Chem. Eur. J.*, 2017, **23**, 15404; G.-X. Jin, M. D. Bailey and M. J. Allen, *Inorg. Chem.*, 2016, **55**, 9085; L. A. Ekanger, L. A. Polin, Y. Shen, E. M. Haacke, P. D. Martin and M. J. Allen, *Angew. Chem. Int. Ed.*, 2015, **54**, 14398; D. N. Huh, C. M. Kotyk, M. Gembicky, A. L. Rheingold, J. W. Ziller and W. J. Evans, *Chem. Commun.*, 2017, **53**, 8664.

13 J. Jiang, N. Higashiyama, K.-i. Machida and G.-y. Adachi, *Coord. Chem. Rev.*, 1998, **170**, 1.

14 D. Wang, C. Zhao and D. L. Phillips, *Organometallics*, 2004, **23**, 1953.

15 G. Scalmani, M. J. Frisch, B. Mennucci, J. Tomasi, R. Cammi and V. Barone, *J. Chem. Phys.*, 2006, **124**, 094107; F. Furche and R. Ahlrichs, *J. Chem. Phys.*, 2002, **117**, 7433; R. E. Stratmann, G. E. Scuseria and M. J. Frisch, *J. Chem. Phys.*, 1998, **109**, 8218; A. D. Becke, *J. Chem. Phys.*, 1993, **98**, 5648; J. P. Perdew, *Phys. Rev. B*, 1986, **33**, 8822.

16 C. A. P. Goodwin, N. F. Chilton, L. S. Natrajan, M.-E. Boulon, J. W. Ziller, W. J. Evans and D. P. Mills, *Inorg. Chem.*, 2017, **56**, 5959; S. Maity and E. Prasad, *J. Photochem. Photobiol., A,* 2014, **274**, 64.

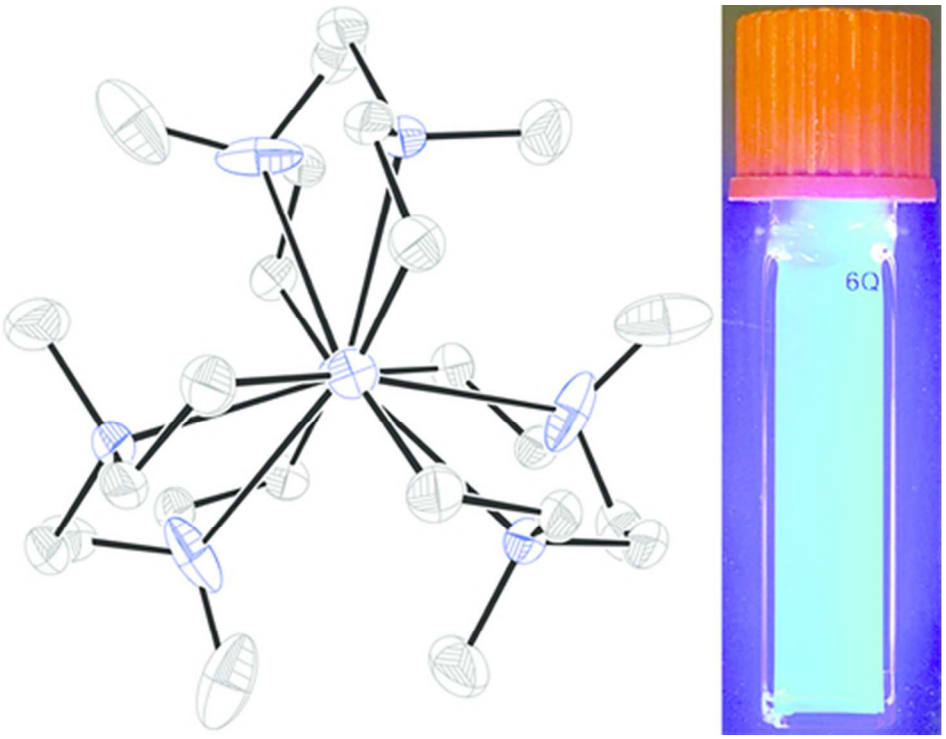


39x30mm (300 x 300 DPI)

Modulation of the coordination environment of europium(II)-containing complexes alters the bright and visible luminescence arising from f–d transitions.